

Article

# The MOND Depth Index and Dynamical Maturity Clock: Toward a Universal Classification of Galaxies and Star Clusters

Robin Eappen <sup>1,\*</sup>  and Pavel Kroupa <sup>1,2,\*</sup> 

<sup>1</sup> Helmholtz-Institut für Strahlen- und Kernphysik (HISKP), Universität Bonn, Nussallee 14-16, 53115 Bonn, Germany

<sup>2</sup> Astronomical Institute, Faculty of Mathematics and Physics, Charles University in Prague, V Holešovickách 2, CZ-180 00 Praha, Czech Republic

\* Correspondence: robin.eappen@gmail.com (R.E.); pkroupa@uni-bonn.de (P.K.)

## Abstract

Mass discrepancies in galaxies are empirically known to appear only below a characteristic acceleration scale  $a_0$ . Here we show that this behaviour is not limited to galaxies: it extends continuously across the full hierarchy of self-gravitating stellar systems, from gas-rich dwarfs and spirals to massive early-type galaxies, and further down to compact stellar clusters. We introduce the—Milgromian dynamics (MOND) depth index  $D_M$ , together with dynamical maturity index  $\mathcal{T} = t_{\text{cross}}/t_H$ , dynamical collisionality index  $\mathcal{T}_1 = t_{\text{cross}}/t_{\text{relax}}$ , with  $t_{\text{cross}}$  being the crossing time,  $t_H$  the Hubble time and  $t_{\text{relax}}$  the median two-body relaxation time, and the MOND acceleration index  $\mathcal{A} = \bar{a}/a_0$ . We uncover a well-defined two-dimensional dividing surface in dynamical space. The ‘dark matter phenomenon’ is found only in systems that are both in the deep-MOND regime ( $\bar{a} < a_0$ ) and collisionless ( $t_{\text{relax}} > t_H$ ), while high-acceleration, collisional systems ( $\bar{a} > a_0$ ,  $t_{\text{relax}} \ll t_H$ ), including globular clusters and UCDs, show no evidence for a mass discrepancy. This clean dynamical separation defines a new, physically motivated classification scheme for stellar systems, unifying galaxies and clusters under one framework. The observed division emerges naturally within the MOND framework and provides a useful diagnostic for examining how different gravitational paradigms account for the origin of the mass discrepancy.

**Keywords:** galaxies; galaxy dynamics; early-types; classification; MOND; clusters

## 1. Introduction

The question of what fundamentally defines a galaxy continues to occupy a central place in modern astrophysics. Since the earliest attempts at classification, astronomers have sought a physical principle capable of organising the wide diversity of observed stellar systems. Jeans [1,2] proposed evolutionary sequences of nebulae within the nebular-hypothesis framework, ideas that later influenced the conceptual basis from which the modern Hubble sequence emerged [3]. Despite their historical importance, such morphological taxonomies remain largely descriptive and do not supply a single physical quantity that captures a galaxy’s structural maturity, dynamical state, or stellar-population age.

A long-standing difficulty in galaxy studies is that many low-mass stellar systems occupy an ambiguous regime in which Newtonian gravity and baryonic matter alone cannot account for the observed kinematics, complicating attempts at a crisp operational definition of a “galaxy”. As emphasised by Willman and Strader [4], a physically meaningful definition should reflect whether a system’s dynamics require physics beyond baryons

arXiv:2603.18135v1 [astro-ph.GA] 18 Mar 2026



Academic Editor: Firstname Lastname

Received: 17 December 2025

Revised: 5 March 2026

Accepted: 11 March 2026

Published:

**Copyright:** © 2026 by the authors.

Licensee MDPI, Basel, Switzerland.

This article is an open access article distributed under the terms and conditions of the [Creative Commons Attribution \(CC BY\) license](https://creativecommons.org/licenses/by/4.0/).

and Newtonian gravity. Several works have therefore argued for definitions based on the underlying dynamical state rather than morphology alone, for example using relaxation time, size, or stellar-population complexity as discriminants [5]. These approaches highlight that galaxies and star clusters form a continuum rather than two clearly separated classes.

More physically motivated definitions have focused on dynamical criteria. A widely discussed operational distinction identifies galaxies as collisionless stellar systems with two-body relaxation times exceeding the Hubble time, as emphasised by Kroupa [6,7]. In this picture, massive globular clusters and ultra-compact dwarfs (UCDs) lie close to the boundary between collisional and collisionless behaviour, whereas dwarf galaxies, spirals, and ellipticals all behave effectively collisionlessly. The degree of virialisation is likewise important: pressure-supported early-type galaxies (ETGs) generally lie close to virial equilibrium (Binney and Tremaine [8]), whereas rotationally supported disks may span a broader range of dynamical maturity. However, neither relaxation time nor virialisation uniquely maps onto stellar age, gas fraction, baryonic compactness, or surface-brightness structure. Dwarf irregulars, low-surface-brightness (LSB) disks, high-surface-brightness (HSB) spirals, and ETGs can exhibit overlapping dynamical timescales despite following distinct evolutionary pathways.

Observational surveys have revealed strong empirical connections between galaxy mass, structural concentration, and stellar-population age. The downsizing phenomenon in which massive ETGs assemble early and quench rapidly is well established (Cowie et al. [9], Thomas et al. [10], Recchi et al. [11], Thomas et al. [12], McDermid et al. [13], Yan et al. [14], Eappen et al. [15], Gjergo and Kroupa [16]). In contrast, many gas-rich dwarf galaxies remain dynamically and chemically unevolved, exhibiting extended star-formation histories and predominantly young stellar populations (Weisz et al. [17], McQuinn et al. [18], Haslbauer et al. [19]). These trends imply a deep connection between stellar age, surface density, and baryonic structure. Yet, they remain fundamentally descriptive: no single scalar quantity predicts a system's position along this evolutionary continuum, and conventional structural parameters (such as Sersic index, effective radius and rotational support) do not unify the full diversity of galaxy types.

From a dynamical perspective, the crossing time and characteristic acceleration provide partial insight. Diffuse galaxies with long crossing times, such as ultra-diffuse or LSB systems are expected to be less dynamically evolved than dense ETGs, which achieve virial equilibrium more rapidly (van Dokkum et al. [20]). However, within the standard  $\Lambda$ CDM framework, baryonic structure does not directly encode dynamical depth: halo concentration, feedback-driven expansion, angular-momentum exchange, and merger history obscure any simple mapping (Bullock and Boylan-Kolchin [21]). In standard dark-matter models, baryonic structure and total dynamical depth are not uniquely coupled, since baryons and dark matter are dynamically distinct components whose relation depends on assembly history and feedback.

Modified Newtonian Dynamics (MOND), originally proposed by Milgrom [22], offers a different perspective. MOND introduces a universal acceleration scale,  $a_0 \approx 1.2 \times 10^{-10} \text{ m s}^{-2}$ , which underpins the baryonic Tully–Fisher relation [23], the radial-acceleration relation [24], and the tight correspondence between baryonic distributions and galaxy kinematics [25]. In its non-relativistic formulation (Bekenstein and Milgrom [26], Milgrom [27]), MOND modifies the Poisson equation such that

$$\nabla \cdot \left[ \mu \left( \frac{|\nabla\Phi|}{a_0} \right) \nabla\Phi \right] = 4\pi G\rho, \quad (1)$$

where  $\Phi$  is the total gravitational potential,  $\rho$  the baryonic density, and  $\mu(x)$  an interpolation function satisfying  $\mu(x) \rightarrow 1$  for  $x \gg 1$  (Newtonian regime) and  $\mu(x) \rightarrow x$  for  $x \ll 1$

(deep-MOND regime), becoming the  $p = 3$  Laplacian field equation, see Scherer et al. [28]. For spherical systems this reduces to the algebraic MOND relation

$$g \mu\left(\frac{g}{a_0}\right) = g_N, \quad (2)$$

where  $g$  is the true gravitational acceleration and  $g_N = GM(r)/r^2$  is the Newtonian value. In the deep-MOND limit ( $g \ll a_0$ ), this yields the space-time scale-invariant form

$$g = \sqrt{g_N a_0} = \sqrt{\frac{GM(r) a_0}{r^2}}. \quad (3)$$

The appearance of the acceleration constant  $a_0$  implies a characteristic MOND radius  $r_M$  (discussed in Section 2, Equation (8), see Milgrom [29]), beyond which internal accelerations fall below  $a_0$  and deep-MOND dynamics dominates. Defined purely by the baryonic mass and a universal constant, this radius delimits the onset of deep-MOND collapse behaviour: compact systems with most of their baryons interior to  $r_M$  evolve rapidly and become dense and old, whereas diffuse systems with most baryons beyond  $r_M$  evolve slowly and remain dynamically young.

These considerations suggest the possibility of a single, physically motivated scalar quantity derived solely from the baryonic distribution relative to the MOND radius that could act as a structural or dynamical ‘clock’ for galaxies. In this work, we develop such an index, which we refer to as the MOND depth index ( $D_M$ ). While its formal definition is presented in Section 2, the basic concept is intuitive: the fraction of a system’s baryons lying in the deep-MOND regime encodes its dynamical depth, collapse history, and likely stellar age. Compact, high-acceleration systems are expected to lie predominantly within  $r_M$  and correspond to old, virialised, quenched galaxies, while diffuse, low-acceleration systems reside deep in the MOND regime and correspond to younger, gas-rich, dynamically unevolved systems. Unlike in  $\Lambda$ CDM, MOND’s universal acceleration scale makes this mapping physically meaningful and potentially predictive.

The purpose of this paper is twofold. First, we introduce a set of physically motivated, MOND-based dynamical diagnostics— $D_M$ ,  $\mathcal{T}$ ,  $\mathcal{T}_1$  and  $\mathcal{A}$ . Each of these depends only on the observed baryonic mass distribution and the characteristic MOND acceleration  $a_0$ . Second, we investigate whether these quantities collectively organise diverse stellar systems, including ETGs from the ATLAS<sup>3D</sup> survey, HSB and LSB spirals, gas-rich dwarfs, and compact clusters/UCDs, into a continuous sequence of structural and dynamical maturity. By comparing  $D_M$ ,  $\mathcal{T}$ ,  $\mathcal{T}_1$  and  $\mathcal{A}$  with stellar ages, gas fractions, internal accelerations, and morphological class, we assess whether a unified, baryonic set of MOND-based diagnostics can reproduce the observed hierarchy of galaxy evolution and simultaneously provide a novel, purely empirical test of MOND itself.

## 2. Dynamical Framework and Definitions

To compare galaxies and stellar clusters within a unified dynamical context, we employ a set of physically motivated quantities that characterize internal timescales, gravitational depth in terms of the degree to which a system resides in the Newtonian or deep-MOND regime (Note: Dwarf satellite galaxies of the Milky Way are in the deep-MOND regime but are not isolated systems: they have typically lost their gas through environmental processes such as ram-pressure or tidal stripping. For this reason, the dynamical indices introduced here are primarily valid for non-satellite galaxies). All quantities are defined using only observable baryonic masses, characteristic radii, and velocity scales, ensuring that the analysis remains baryon-based.

The first fundamental quantity is the dynamical or crossing time, which measures the characteristic time for an object to traverse the system. For pressure-supported systems, we adopt

$$t_{\text{cross}} = \frac{2R}{\sigma}, \quad (4)$$

where  $R$  is a representative radius (typically the half-light or effective radius; see Hernquist [30], Cappellari et al. [31]) and  $\sigma$  is the line-of-sight velocity dispersion. For rotationally supported systems we analogously define

$$t_{\text{cross}} = \frac{\pi R}{V_c}, \quad (5)$$

using the circular velocity  $V_c$  measured at a characteristic radius (e.g., Lelli et al. [32]). Compact systems therefore exhibit short crossing times and rapid internal evolution, while diffuse galaxies have long dynamical times and evolve slowly.

Another fundamental time scale characterizing gravitationally bound stellar systems is the classical median two-body relaxation time, which quantifies the timescale on which stellar encounters redistribute energy. For a system of  $N$  equal-mass stars with characteristic stellar mass  $M_*$  and half-mass radius  $R_h$ , we adopt the standard approximation (Binney and Tremaine [33])

$$t_{\text{relax}} \approx \frac{0.1 N}{\ln(0.4N)} t_{\text{cross}}. \quad (6)$$

Following the arguments of Kroupa [6], Dabringhausen et al. [34] and with  $t_H$  being the Hubble time, systems with  $t_{\text{relax}} > t_H$  behave effectively as collisionless galaxies, while systems with  $t_{\text{relax}} < t_H$  are collisional and dynamically evolve as star clusters. Relaxation and virialisation must be clearly distinguished: a system may satisfy the virial theorem,

$$2K + W = 0, \quad (7)$$

after only a few crossing times, yet still possess a relaxation time far exceeding the Hubble time. Galaxies are therefore virialised but collisionless objects, whereas globular clusters and some UCDs can be both virialised and older than one median two-body relaxation time (Meylan and Heggie [35]).

A central element of our analysis is the internal gravitational acceleration compared to the ubiquitous MOND acceleration constant  $a_0$  discovered by Milgrom [22]. MOND introduces a characteristic scale that marks the transition between Newtonian and scale-invariant deep-MOND dynamics. For a system of baryonic mass  $M_{\text{bar}}$ , one may define a MOND radius by equating the Newtonian acceleration  $GM_{\text{bar}}/r^2$  with  $a_0$ :

$$r_M = \sqrt{\frac{GM_{\text{bar}}}{a_0}}. \quad (8)$$

This radius, implicit in Milgrom's original formulation and made explicit in later MOND analyses (e.g., Famaey and McGaugh [36]), identifies the scale beyond which internal accelerations fall below  $a_0$  and deep-MOND behaviour dominates. Systems whose baryonic mass lies predominantly inside  $r_M$  are expected to undergo rapid early collapse and become dynamically compact and old, whereas systems with a large fraction of their baryons outside  $r_M$  evolve in the low-acceleration regime and therefore are expected to collapse more slowly (e.g., Sanders [37], Kroupa et al. [38]).

To quantify how deeply a system resides in the MOND regime, we introduce the *MOND depth index*

$$D_M = 1 - \frac{M(< r_M)}{M_{\text{bar}}}, \quad (9)$$

where  $M(< r_M)$  is the baryonic mass enclosed within the MOND radius. In this work, the enclosed mass is computed from analytic profiles matched to each galaxy type: for ETGs we assume a Hernquist profile [30] with scale length  $a = R_e/1.8153$ , where  $R_e$  is the effective radius, while for rotationally supported SPARC disks and dwarfs we adopt an exponential disk with scale length  $R_d$ . The quantity  $D_M$  ranges from  $D_M \approx 0$  for compact, Newtonian-like systems to  $D_M \approx 1$  for diffuse, deep-MOND systems. Because  $D_M$  depends solely on the baryonic mass distribution and the universal constant  $a_0$ , it provides an observationally accessible measure of gravitational depth and structural maturity applicable across all galaxy types (e.g., Haslbauer et al. [19], Lelli et al. [24]).

A second key quantity is the dimensionless dynamical maturity index,

$$\mathcal{T} = \frac{t_{\text{cross}}}{t_H}, \quad (10)$$

which measures the number of internal dynamical cycles a system has experienced over the age of the Universe. Systems with  $\mathcal{T} \ll 1$  have undergone many internal dynamical cycles and are dynamically old (e.g., ETGs), while systems with  $\mathcal{T}$  approaching unity have experienced only a few crossing times and remain dynamically young (e.g., LSB disks and diffuse dwarfs).  $\mathcal{T}$  is well defined for both pressure-supported and rotationally supported systems, making it particularly well suited to the broad comparative analysis pursued here.

A long-standing dynamical criterion is that galaxies should behave as collisionless stellar systems, with two-body relaxation times exceeding the Hubble time [5] (see their discussion on using relaxation time as a galaxy-defining property). This motivates the inclusion of the dynamical collisionality index

$$\mathcal{T}_1 = \frac{t_{\text{cross}}}{t_{\text{relax}}}, \quad (11)$$

which measures how many crossing times occur per relaxation time in our diagnostic framework. This ratio therefore provides a convenient, morphology independent description between galaxies (collisionless) and star clusters (collisional), complementing earlier work by Kroupa [6], Dabringhausen et al. [34].

Finally, to characterise gravitational depth in a morphology-independent manner, we define a mean internal acceleration

$$\bar{a} = \frac{GM_{\text{bar}}}{R_e^2}, \quad (12)$$

and normalise it by the MOND acceleration constant to form another dimensionless index which we define as the acceleration index,

$$\mathcal{A} = \frac{\bar{a}}{a_0}. \quad (13)$$

Large values of  $\mathcal{A}$  correspond to compact, dynamically deep systems that lie predominantly inside  $r_M$ , whereas small values identify diffuse systems operating well within the deep-MOND regime (e.g., Famaey and McGaugh [36], Kroupa et al. [38], McGaugh and Milgrom [39]).

Together, these indices  $D_M$ ,  $\mathcal{T}$ ,  $\mathcal{T}_1$ , and  $\mathcal{A}$  provide a coherent and fully baryonic set of dynamical descriptors applicable across the entire hierarchy of stellar systems. These

indices form the basis for the diagnostic planes introduced in Section 4, where they reveal a continuous dynamical sequence connecting star clusters, dwarfs, spirals, and ETGs.

### 3. Data and Sample Selection

To assess whether the  $D_M$  provides a unified dynamical description across the full hierarchy of stellar systems, we assemble a heterogeneous but well characterized sample drawn from major observational surveys and literature catalogs. The combined dataset spans ETGs, HSB and LSB spirals and dwarfs, compact stellar systems, including globular clusters and UCDs. The inclusion of compact stellar systems is particularly important because UCDs and massive globular clusters extend smoothly into the parameter space of dwarf galaxies, forming a continuous size–mass sequence [40]. This structural continuity reinforces the need for a unified dynamical diagnostic applicable across the full hierarchy of stellar systems. A summary of the datasets and the key quantities used in our analysis is provided in Table 1. For every system we compile baryonic masses, characteristic radii, velocity scales, and, where possible, stellar-population ages. These observables allow a homogeneous computation of the dynamical quantities defined in Section 2, including crossing times, relaxation times, internal accelerations, MOND radii, and the  $D_M$ .

**Table 1.** Summary of the datasets used in this study.

Dataset/Type	Mass	Radius	Age
ATLAS <sup>3D</sup> (ETGs)	$M_*$ (Cappellari et al. [31])	$R_e$ (Cappellari et al. [31])	luminosity-weighted ages (McDermid et al. [13])
SPARC (disks & dwarfs)	$M_*$ , $M_{\text{gas}}$ (Lelli et al. [32])	$R_d$ (Lelli et al. [32])	$t_{\text{gas}}$ (Equation (15))
MCO (GCs, UCDs, etc.)	$M_{\text{dyn}}$ (Dabringhausen et al. [34])	$R_h$	old ( $\geq 10$ –12 Gyr)

Note. For ATLAS<sup>3D</sup> early-type galaxies we use stellar masses, effective radii, and luminosity-weighted ages from the indicated references. For SPARC disks and dwarfs we adopt stellar and gas masses (including helium), exponential scale lengths, and gas-consumption ages  $t_{\text{gas}}$ . For MCOs we use dynamical masses and half-light radii from the literature. These quantities provide the inputs for computing the  $D_M$ ,  $\mathcal{T}$ ,  $\mathcal{T}_1$  and  $\mathcal{A}$  across all stellar systems.

The ETG component is drawn primarily from the ATLAS<sup>3D</sup> survey (Cappellari et al. [31]), which provides homogeneous integral-field spectroscopy, photometry, and dynamical modelling for 260 nearby ETGs. For the present analysis, we select those ETGs with published luminosity-weighted stellar ages from McDermid et al. [13], ensuring a consistent treatment of stellar populations. Effective radii, stellar masses, and velocity dispersions are taken from Cappellari et al. [41], providing the necessary inputs for computing  $t_{\text{cross}}$ ,  $\bar{a}$ , and  $r_M$  under the baryonic framework adopted here.

Rotationally supported spirals and dwarfs are taken from the SPARC database [32], which provides high-quality rotation curves and H I measurements for 175 galaxies covering the full range of disk morphologies and surface brightnesses, from HSB spirals to extremely diffuse, gas-rich dwarfs. From SPARC we adopt stellar masses, gas masses (multiplied by 1.33 to include helium; McGaugh and de Blok [42]), exponential disk scale lengths, and characteristic circular velocities  $V_c$ .

We use the sample of Massive Compact Objects (MCOs) from Tables 1 and 2 of Dabringhausen et al. [34] (also referred to as D08), which includes globular clusters, UCDs, and intermediate compact systems with published dynamical mass estimates, half-light radii, and internal velocity dispersions. Following their classification, we treat all these objects uniformly as MCOs. Although such systems are collisional on long timescales (Meylan and Heggie [35]), their inclusion enables us to test whether  $D_M$  can connect collisional star clusters and collisionless galaxies along a single continuous dynamical

sequence as an extension of the traditional relaxation-based classifications (Forbes and Kroupa [5], Kroupa [6]).

For the SPARC galaxies we estimate a simple gas-consumption age rather than adopting literature stellar ages, which are not homogeneously available for the full sample. Conceptually, a gas-consumption timescale may be written as  $t_{\text{gas}} \approx M_{\text{gas}}/\text{SFR}$  (e.g. Kennicutt [43]). In practice, we lack SFR measurements for many SPARC galaxies, so we approximate  $t_{\text{gas}}$  using the global gas fraction,

$$f_{\text{gas}} = \frac{M_{\text{gas}}}{M_{\text{gas}} + M_{\star}}, \quad (14)$$

and assume an exponential gas-depletion law with a characteristic depletion timescale  $\tau_{\text{dep}} = 3 \text{ Gyr}$ , consistent with typical values for nearby star-forming disks (Haslbauer et al. [19], Leroy et al. [44]). Under these assumptions the gas fraction evolves as  $f_{\text{gas}} \propto \exp(-t/\tau_{\text{dep}})$ , which implies for the time to reach a fraction  $1/e$  of  $f_{\text{gas}}$

$$t_{\text{gas}} = -\tau_{\text{dep}} \ln f_{\text{gas}}. \quad (15)$$

We compute this quantity for all SPARC galaxies with  $0 < f_{\text{gas}} < 1$ , and clip the resulting ages at the Hubble time  $t_H = 13.8 \text{ Gyr}$ . All systems considered are local ( $z \approx 0$ ); thus, we adopt the present-day Hubble time. A redshift-dependent  $t_H(z)$  would not alter the qualitative ordering. These  $t_{\text{gas}}$  values should not be interpreted as physical stellar ages; they serve only as relative indicators of evolutionary state (e.g. young, gas-rich dwarfs versus older, gas-poor spirals). Importantly, they play no role in the computation of the dynamical quantities  $D_M$ ,  $\mathcal{T}$ ,  $\mathcal{T}_1$  or  $\mathcal{A}$ . These toy ages are used purely for visual colour-coding and do not enter any dynamical computation.

The same SPARC catalogue is used to divide galaxies into four broad morphological surface brightness classes: HSB spirals, LSB spirals, HSB dwarfs, and LSB dwarfs. We use the de Vaucouleurs  $T$ -type to distinguish dwarfs from spirals, adopting  $T \geq 7$  (Sd, Sm, Im, Blue Compact Dwarf) as dwarfs and  $T < 7$  as spirals, and we classify discs as LSB when  $\log_{10} SB_{\text{disk}} < 2.5$ , corresponding to a central surface brightness of  $\approx 300 L_{\odot} \text{ pc}^{-2}$  (see Lelli et al. [32]). Galaxies with non-finite  $SB_{\text{disk}}$  values are conservatively assigned to the LSB class. This four-way division is used for plotting and for visualising where different morphological families lie in the diagnostic planes.

Figure 1 illustrates the distribution of the gas-consumption ages,  $t_{\text{gas}}$ , as a function of baryonic mass for the SPARC galaxies. Low-mass and LSB dwarfs typically have  $t_{\text{gas}} \leq 2 \text{ Gyr}$ , reflecting their high gas fractions and slow, prolonged star-formation histories and youth (Haslbauer et al. [19], McGaugh and de Blok [42], Hunter and Elmegreen [45], Weisz et al. [46]). HSB spirals, by contrast, exhibit substantially older gas-consumption ages, often 6–12 Gyr, consistent with more evolved stellar populations, higher stellar-to-gas ratios, and earlier formation epochs (Bell and de Jong [47], Gallazzi et al. [48], Leroy et al. [44]). These trends are in line with the broader picture that diffuse, low-acceleration galaxies remain chemically and dynamically unevolved, whereas massive disks form the bulk of their stars at earlier cosmic times.

Stellar ages for ETGs are taken directly from McDermid et al. [13], who provide luminosity-weighted ages derived from full spectral fitting. For SPARC galaxies we rely exclusively on the gas-consumption ages described above; we do not mix these with heterogeneous stellar ages from the literature. For MCOs we do not compute ages explicitly; instead, they are treated as old systems with typical ages  $\geq 10$ –12 Gyr (Dabringhausen et al. [34]) and are shown in the diagnostic planes with a fixed symbol that is not tied to the colour-coded age scale.

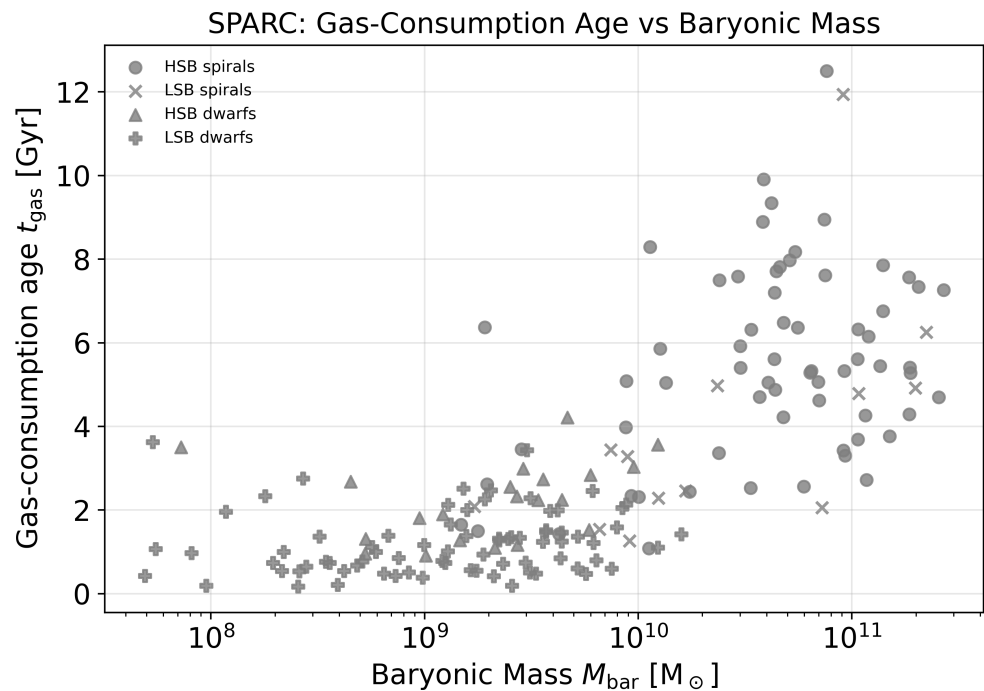


**Figure 1.** The gas-consumption age  $t_{\text{gas}}$  as a function of baryonic mass for the SPARC galaxies, estimated from the gas fraction assuming an exponential depletion law with  $\tau_{\text{dep}} = 3 \text{ Gyr}$ . LSB dwarfs populate the youngest part of the distribution, while HSB spirals show substantially older gas-consumption ages. This behaviour reflects the extended star-formation histories and high gas fractions characteristic of diffuse, low-acceleration systems.

All radii, masses, and velocities are homogenized through consistent unit conversions and, where necessary, matched definitions across the heterogeneous sample. For each object in the combined catalogue we compute the crossing time, relaxation time, mean acceleration, MOND radius, and all the dynamical indices introduced in this paper using the definitions in Section 2. The final sample spans nearly eight orders of magnitude in baryonic mass and covers the full observed range of surface brightnesses. This broad dynamical baseline makes it ideally suited to testing whether the  $D_M$  defined entirely from baryonic quantities captures the structural and evolutionary organisation of stellar systems across the entire mass spectrum. The final combined sample contains  $N_{\text{ETGs}} = 258$  ETGs,  $N_{\text{SPARC}} = 175$  SPARC galaxies, and  $N_{\text{MCOs}} = 32$  MCOs.

#### 4. Results: Dynamical Diagnostic Planes

Using the dynamical quantities introduced in Section 2, we construct three complementary diagnostic planes that jointly characterise the collisionality, dynamical maturity, acceleration regime and MOND depth of ETGs, HSB and LSB—spirals and dwarfs and MCOs. Although these systems span more than eight orders of magnitude in mass and exhibit diverse morphologies, they occupy coherent and physically interpretable loci in all three diagnostic planes. Taken together, these planes reveal a continuous dynamical sequence that links galaxies and star clusters through their internal accelerations, crossing times, and positions relative to the MOND radius. Below we discuss each diagnostic plane in turn, starting from the most fundamental dynamical division and moving toward structurally motivated MOND quantities.

##### 4.1. $\mathcal{T}_1$ vs. $\mathcal{A}$

Figure 2 compares collisionality index,  $\mathcal{T}_1$  with the acceleration index,  $\mathcal{A}$ . Because the relaxation time scales as  $t_{\text{relax}} \propto N t_{\text{cross}}$ , this ratio serves as a direct measure of collisionality:

large values identify systems where two-body encounters drive evolution, while small values correspond to collisionless dynamics.

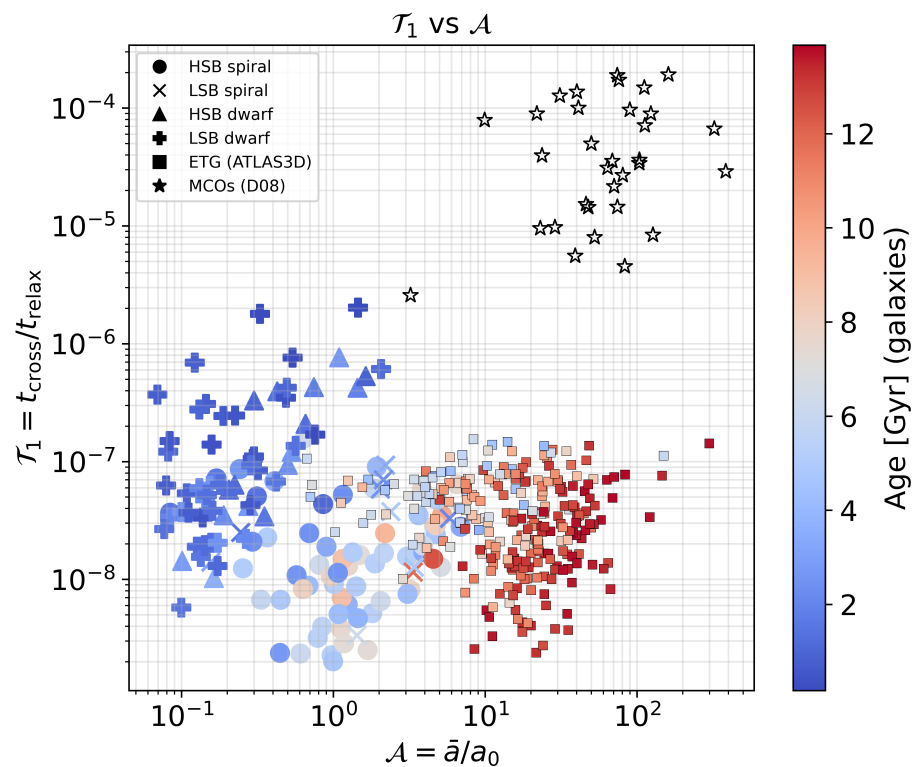


**Figure 2.** Collisionality index,  $\mathcal{T}_1$  as a function of acceleration index,  $\mathcal{A}$ . The diagnostic cleanly separates collisional stellar systems (MCOs) from collisionless galaxies. The colour bar depicts the age ( $t_{\text{age}}$  values and other as defined in Section 3).

MCOs occupy the high- $\mathcal{T}_1$  region of the diagnostic plane, reflecting their collisional nature. More massive MCOs and compact ellipticals lie near the classical relaxation boundary  $t_{\text{relax}} \approx t_H$ , confirming that these objects inhabit the transitional regime previously discussed in Kroupa [6] and Dabringhausen et al. [34]. All galaxies: ETGs, HSB and LSB—spirals and dwarfs lie far below this boundary across the full range of accelerations probed. This diagnostic plane therefore recovers the fundamental physical distinction between galaxies and MCOs, and it does so through a purely dynamical plane that naturally incorporates the MOND acceleration scale.

#### 4.2. $\mathcal{T}$ vs. $\mathcal{A}$

Figure 3 shows  $\mathcal{T}$  as a function of  $\mathcal{A}$ . Unlike the relaxation time, which diverges for collisionless galaxies and therefore cannot serve as a universal dynamical age indicator, the Hubble time provides a finite and uniform reference scale.  $\mathcal{T}$  is therefore well-defined for all systems, from MCOs to giant ETGs.

MCOs occupy the extreme high-acceleration regime with  $\mathcal{T} \approx 0$ , reflecting their extremely short dynamical timescales. ETGs also lie at high  $\mathcal{A}$  but exhibit moderately small  $\mathcal{T}$ , consistent with early formation and long-term dynamical stability. Spirals span an intermediate range in both variables, while diffuse dwarfs populate the lowest-acceleration end but do not achieve large  $\mathcal{T}$ ; their small sizes yield relatively short crossing times despite being deep-MOND systems.

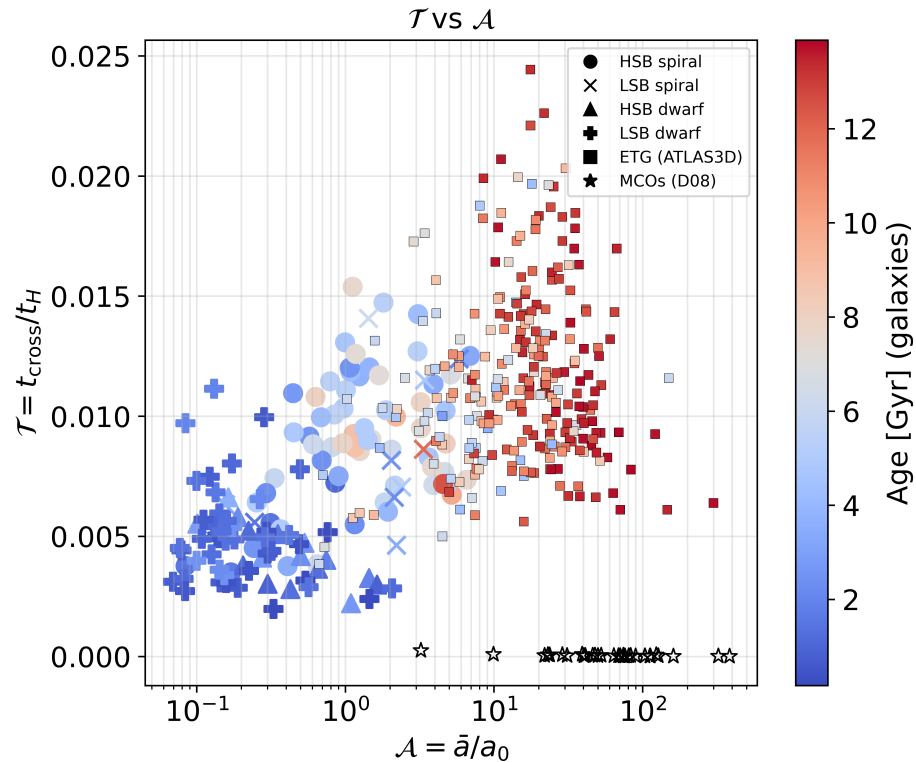


**Figure 3.** Dynamical maturity index,  $\mathcal{T}$  as a function of  $\mathcal{A}$ . A continuous acceleration–timescale sequence links all galaxy types and MCOs. The vertical axis is shown on a linear scale to highlight the relative spread in  $\mathcal{T}$  among the galaxy populations; MCOs, which occupy a very narrow range in  $\mathcal{T}$ , therefore appear cluttered near the lower edge of the diagnostic plane. The colour bar is as in Figure 2.

The combined distribution reveals that neither morphology nor total mass sets a galaxy’s dynamical age. Instead,  $\mathcal{A}$  serves as the primary organising index: self-gravitating systems follow a broad structural progression in the  $(\mathcal{T}-\mathcal{A})$  plane, with compactness (or internal acceleration) regulating crossing times rather than the MOND regime itself. Overall, the  $(\mathcal{T}-\mathcal{A})$  plane reveals a structural hierarchy rather than a monotonic evolutionary sequence: dynamical age is primarily governed by internal compactness, with  $\mathcal{A}$  acting as the unifying index across galaxies and star clusters. This plane demonstrates that dynamical age is not determined by galaxy mass or morphology. Instead, internal acceleration (compactness) acts as the primary organising index.

#### 4.3. $D_M$ vs. $\mathcal{T}$

Figure 4 compares the  $D_M$  a structural measure of how deeply a system lies inside its MOND radius with the dynamical maturity index,  $\mathcal{T}$ . Although these two quantities are derived from related but distinct definitions of dynamical depth within the MOND framework, the diagnostic plane formed displays a remarkably well-defined sequence.

ETGs and MCOs occupy the region of low  $D_M$  and low  $\mathcal{T}$ , indicating deep potential wells and dynamically old configurations. HSB spirals bridge the gap toward higher  $D_M$ , while LSB galaxies and diffuse dwarfs populate the opposite extreme of large  $D_M$  and large  $\mathcal{T}$ , reflecting shallow gravitational potentials and slow dynamical evolution. (Although diffuse dwarfs lie in the deep-MOND regime (large DM), their small physical sizes prevent  $\mathcal{T}$  from reaching the extreme values seen in larger diffuse disks.)

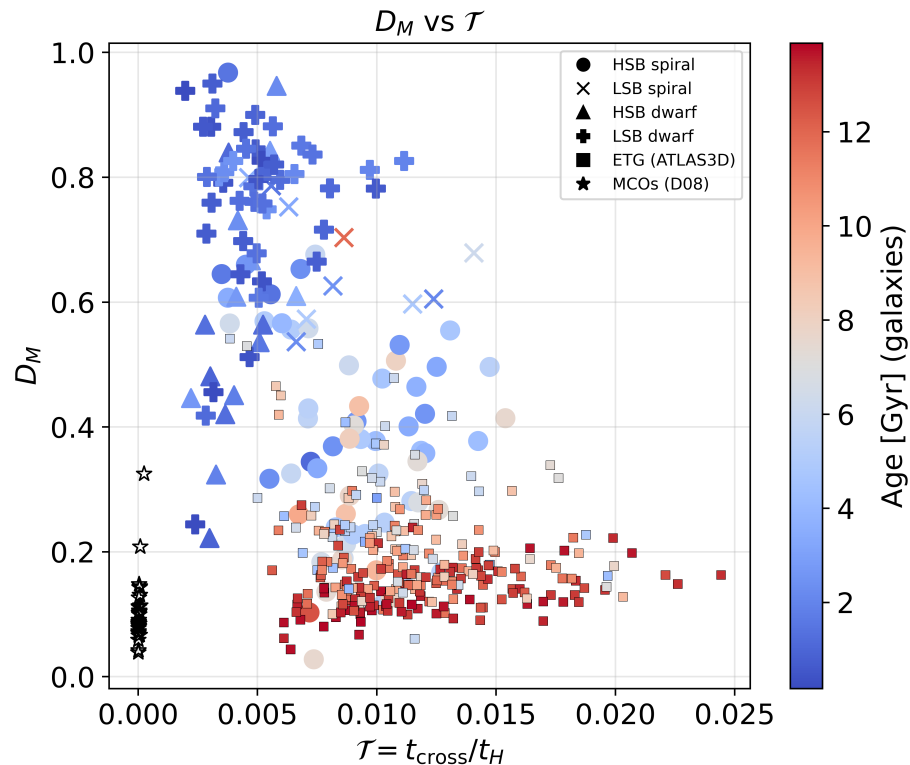


**Figure 4.** MOND depth index,  $D_M$  versus dynamical maturity index,  $\mathcal{T}$ , colour-coded by stellar population age. A continuous sequence emerges that links structural depth, dynamical maturity, and stellar age across all galaxy types. A linear scale is adopted for the  $\mathcal{T}$ -axis to enhance the visual spread of the galaxy populations along the horizontal direction; as a consequence, the MCOs, which occupy a very narrow range in  $\mathcal{T}$ , appear visually cluttered near the left edge of the diagnostic plane. The colour bar is as in Figure 2.

When colour-coded by stellar population age, the sequence becomes an evolutionary axis: dynamically deep systems are old, while dynamically shallow systems are young. Thus,  $D_M$  and  $\mathcal{T}$  jointly encode both the structural maturity and collapse history of stellar systems, providing a dynamical explanation for downsizing trends in galaxy populations.

## 5. Discussion

The diagnostic planes presented in Section 4 demonstrate that self-gravitating stellar systems across the full observable hierarchy from diffuse dwarfs and LSB disks to massive ETGs, HSB spirals and MCOs populate a remarkably continuous and physically interpretable set of sequences. Despite spanning eight orders of magnitude in baryonic mass, and exhibiting a wide range of structural and kinematic properties, these systems align in a manner that is naturally organised by  $D_M$ ,  $\mathcal{T}$ ,  $\mathcal{A}$ , and  $\mathcal{T}_1$ . Taken together, these relations define an empirical dynamical backbone that links structural depth, collapse history, and stellar age across all classes of stellar systems. The continuous behaviour seen in our MOND-based diagnostic planes reflects the structural continuity long recognised between MCOs (which includes massive globular clusters and UCDs) and dwarf galaxies [40]. This supports the view that these systems trace a single underlying sequence rather than representing sharply distinct classes.

A central result is that galaxies and MCOs form a unified dynamical sequence when expressed in the  $(D_M, \mathcal{T})$  plane. Low- $D_M$  systems (ETGs and MCOs) exhibit short crossing times, high accelerations, and old stellar populations, consistent with early and rapid collapse (e.g. Thomas et al. [10], McDermid et al. [13], Yan et al. [14], Eappen et al. [15], van

Dokkum et al. [49]). At the opposite extreme, diffuse dwarfs and LSB spirals reside at large  $D_M$  and large  $\mathcal{T}$ , reflecting their shallow potentials, slow collapse, and young or extended star-formation histories (e.g. Haslbauer et al. [19]). HSB spirals bridge these two populations with intermediate MOND depths and dynamical ages, forming the central spine of the overall sequence.

The colour-coding by stellar population age further shows that this dynamical sequence is simultaneously an evolutionary sequence: dynamically deep systems are predominantly old, while dynamically shallow systems are young. In this sense, the  $D_M$  provides a physical underpinning for the well-established phenomenon of downsizing (Cowie et al. [9], Thomas et al. [10], Yan et al. [14], Eappen et al. [15]), long recognised in observational studies of galaxy evolution. Within the MOND framework, this behaviour emerges naturally from the scaling of the MOND radius  $r_M \propto M_{\text{bar}}^{1/2}$  and from the sensitivity of collapse times to internal acceleration: massive galaxies collapse within  $r_M$ , achieving high accelerations and quickly quenching, whereas low-mass, diffuse systems form and evolve in the deep-MOND regime with prolonged dynamical and star-forming timescales (Sanders [37], Kroupa et al. [38], Banik and Zhao [50]). In standard dark-matter based models, the relation between baryonic structure and total dynamical depth depends on halo concentration, assembly history, and baryon–halo coupling, which introduce additional degrees of freedom and scatter (e.g. Disney et al. [51]).

In addition to dark-matter based and MOND frameworks, a number of purely Newtonian models that explicitly account for realistic galaxy geometry (e.g., disk or oblate mass distributions) have been explored in the literature (e.g., Feng [52], Hofmeister and Criss [53,54]). These studies consider whether detailed Newtonian force balance using baryonic mass distributions alone can reproduce aspects of observed rotation curves, and we include this acknowledgment here for completeness.

The  $\mathcal{T}_1$  versus  $\mathcal{A}$  plane recovers, with modern data, the classical collisionless–collisional divide originally emphasised by Kroupa [6] and extended in Dabringhausen et al. [34]. MCOs occupy the collisional regime, while all galaxies irrespective of morphology or mass lie securely within the collisionless domain. The addition of the MOND acceleration axis sharpens this boundary by showing that high-acceleration, compact stellar systems approach the relaxation threshold from above, whereas diffuse galaxies remain far below it. ETGs likely reach quasi-equilibrium via rapid collective processes such as violent relaxation and dissipative gas collapse, rather than via two-body relaxation.

Several systematic uncertainties must be acknowledged. The definition of the characteristic radius differs somewhat across ETGs, spirals, and dwarfs; while these choices follow standard practice (e.g., Cappellari et al. [31], Lelli et al. [32]), they introduce scatter in both  $\bar{a}$  and  $t_{\text{cross}}$ . Stellar ages for gas-rich dwarfs are uncertain and often spatially variable, which may blur the age–dynamics correspondence at low mass. The computation of  $M(< r_M)$  relies on Hernquist or exponential approximations that, while reasonable, cannot capture all structural diversity, especially for disturbed or composite systems. Finally, some MCOs may host massive central black holes (Seth et al. [55]) or sub-clusters of stellar-mass black holes (Mahani et al. [56]), which could influence their internal accelerations. Yet despite these uncertainties, the observed dynamical sequences remain strikingly well defined, suggesting that the key physical trends are robust.

The dynamical diagnostic planes introduced in this work occupy a conceptual role somewhat analogous to that of the Hertzsprung–Russell (HR) diagram for stars (Hertzsprung [57], Russell [58]). The classical HR diagram provides a unified framework in which stars populate distinct, physically interpretable sequences whose positions reflect their internal structure and evolutionary state. In an analogous, though not identical, manner our diagnostic planes show that galaxies and stellar clusters do not populate the

dynamical indices space randomly: HSB and LSB spirals and dwarfs, ETGs and MCOs all occupy well-defined and contiguous regions in the planes defined by  $D_M$ ,  $\mathcal{T}$ ,  $\mathcal{T}_1$ , and  $\mathcal{A}$ . The location of a system in these planes encodes its dynamical maturity, internal acceleration regime, compactness, and collisional state, thereby offering a unified classification scheme across the full hierarchy of stellar systems. Extending this framework to galaxy groups and clusters would provide an important test, particularly given the known residual mass discrepancy in MOND at cluster scales has recently been amended [59].

The emergence of continuous sequences from deep-MOND, dynamically old ETGs to diffuse, dynamically young LSB disks, and further to relaxation-dominated MCOs demonstrates that these planes provide a useful structural–dynamical analogue to the HR diagram. They thus offer a new way to characterise galaxies in terms of their dynamical state and evolutionary maturity within the MOND framework. Overall, the  $D_M$  and  $\mathcal{T}$  together provide a simple, baryon-based, and physically grounded framework for understanding the internal dynamics, structural maturity, and evolutionary pathways of stellar systems. The continuity of the sequences uncovered here indicates that galaxies and MCOs form a dynamically ordered family rather than a set of disjoint morphological categories. In this sense,  $D_M$  and  $\mathcal{T}$  together define a physically motivated dynamical classification framework that organises stellar systems across a wide range of mass and morphology.

## 6. Conclusions

In this work we have introduced a new, physically motivated dynamical index,  $D_M$ , defined purely from the baryonic mass distribution and the universal MOND acceleration scale  $a_0$ . Together with  $\mathcal{T}$ ,  $\mathcal{T}_1$  and  $\mathcal{A}$ , these indices provide a compact description of dynamical depth, collapse history, and internal gravitational regime for stellar systems across the full mass spectrum.

Using a combined sample of ETGs from ATLAS<sup>3D</sup>, spirals and dwarfs from SPARC and compact stellar systems from Dabringhausen et al. [34], we have shown that stellar systems occupy a continuous dynamical sequence in the primary diagnostic planes defined by  $(D_M, \mathcal{T})$ ,  $(\mathcal{T}, \mathcal{A})$ , and  $(\mathcal{T}_1, \mathcal{A})$  (A supplementary structural trend between  $D_M$  and total baryonic mass is presented in Appendix A). Dynamically deep systems with small  $D_M$  (ETGs and compact stellar systems) are universally old, while dynamically shallow systems with high  $D_M$  (LSB disks and diffuse dwarfs) are young and gas-rich. This provides a baryonic dynamical framework consistent with the observed downsizing phenomenon (Cowie et al. [9], Thomas et al. [10,12], McDermid et al. [13], Yan et al. [14]), linking stellar-population age directly to  $D_M$ ,  $\mathcal{T}$  and  $\mathcal{A}$ .

The  $(\mathcal{T}_1, \mathcal{A})$  plane naturally recovers the classical “galaxy versus star-cluster” boundary proposed by Kroupa [6] and extended by Dabringhausen et al. [34]: all galaxies occupy the collisionless regime with  $t_{\text{relax}} > t_H$ , while MCOs lie in the collisional regime. The MOND radius  $r_M$  provides a physically meaningful collapse scale: systems with most of their baryons inside  $r_M$  tend to exhibit short dynamical times and old stellar populations, whereas systems with most of their baryons outside  $r_M$  evolve more slowly in the deep-MOND regime.

Taken together, these findings demonstrate that  $D_M$ ,  $\mathcal{T}$ ,  $\mathcal{T}_1$  and  $\mathcal{A}$  provide a powerful and unified framework for understanding structural evolution, dynamical evolution, and stellar-population age across the full spectrum of stellar systems. The coherence of the resulting sequences, and their connection to stellar ages, illustrate how the MOND framework provides a natural context for organising structural and dynamical trends across stellar systems. Future work should extend this analysis to larger and higher-redshift samples, including JWST galaxies, ultra-diffuse systems in diverse environments, and massive

compact objects, in order to test the robustness and universality of the  $D_M$ -based dynamical classification proposed here.

**Author Contributions:** R.E. developed the initial concept of the MOND depth index and performed all calculations and data analysis. P.K. contributed to the development of the dynamical-age indicator  $\mathcal{T}$  and advised on the connection between the acceleration ratio and relaxation time. R.E. prepared the first draft of the manuscript; R.E. and P.K. jointly revised and developed the manuscript. All authors have read and agreed to the published version of the manuscript.

**Funding:** This work is not part of a funded project.

**Data Availability Statement:** The original contributions presented in this study are included in the article/supplementary material. Further inquiries can be directed to the corresponding author(s).

**Acknowledgments:** The author R.E. would like to thank KFPP for their support. P.K. would like to thank the DAAD Bonn—Eastern European Exchange program at the University of Bonn and Charles University in Prague for support. The authors thank J. Dabringhausen for suggesting the connection between the acceleration ratio and the relaxation-timescale condition for collisional systems, which helped refine the interpretation of the dynamical sequence.

**Conflicts of Interest:** The authors declare no conflicts of interest.

## Appendix A. Supplementary Structural Trend: $D_M$ versus Baryonic Mass

For completeness, we illustrate in Figure A1 the empirical relation between the MOND depth index  $D_M$  and the total baryonic mass of the systems considered.

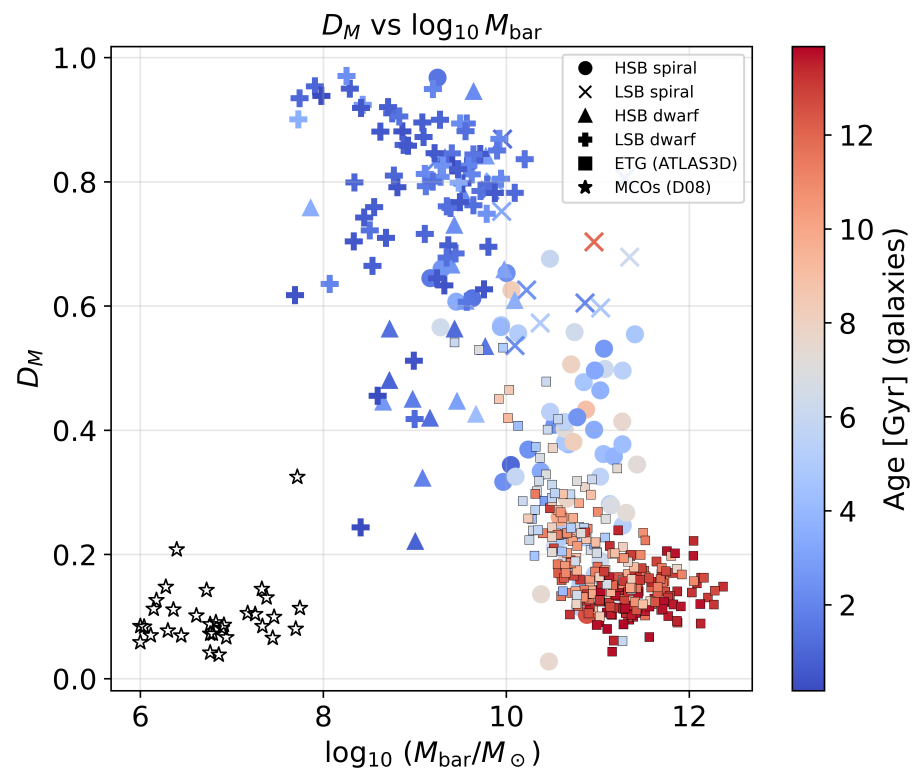


**Figure A1.** MOND depth index  $D_M$  as a function of total baryonic mass. The relation reflects the scaling of the MOND radius  $r_M \propto M_{\text{bar}}^{1/2}$ , shown here for completeness as a supplementary structural trend within the sample. The colour bar is as in Figure 2.

Low-mass dwarf systems tend to occupy the regime  $D_M \approx 1$ , indicating that a large fraction of their baryons lie outside their MOND radius. Intermediate-mass spiral galaxies populate a transitional region, while early-type galaxies and compact stellar

systems generally exhibit  $D_M \ll 1$ , consistent with higher internal accelerations and greater baryonic concentration within  $r_M$ .

Since the MOND radius scales as  $r_M \propto M_{\text{bar}}^{1/2}$ , a systematic variation of  $D_M$  with mass is expected at the level of dimensional scaling. We emphasise, however, that this relation should not be interpreted as a strict mass threshold or universal boundary. Known extended low-surface-brightness systems and galaxy groups demonstrate that structural depth depends not only on total mass but also on the spatial distribution of baryons.

We therefore present this plane as a supplementary structural trend within the present dataset, rather than as a primary diagnostic. The main results of this work remain the dynamical classification planes involving  $\mathcal{A}$ ,  $\mathcal{T}$ , and  $D_M$  discussed in Section 4.

## References

1. Jeans, J.H. Problems of Cosmogony and Stellar Dynamics. *JSTOR* **1919**, *18*, 674–678.
2. Jeans, J.H. *Astronomy and Cosmogony*; Cambridge University Press: Cambridge, UK, 1928. <https://doi.org/10.1017/CBO9780511694363>.
3. Hubble, E.P. Extragalactic nebulae. *Astrophys. J.* **1926**, *64*, 321–369. <https://doi.org/10.1086/143018>.
4. Willman, B.; Strader, J. “Galaxy,” Defined. *Astron. J.* **2012**, *144*, 76. <https://doi.org/10.1088/0004-6256/144/3/76>.
5. Forbes, D.A.; Kroupa, P. What Is a Galaxy? Cast Your Vote Here. *Publ. Astron. Soc. Aust.* **2011**, *28*, 77–82. <https://doi.org/10.1071/AS10029>.
6. Kroupa, P. The dynamical evolution of stellar superclusters. *Mon. Not. R. Astron. Soc.* **1998**, *300*, 200–204. <https://doi.org/10.1046/j.1365-8711.1998.01892.x>.
7. Kroupa, P. Initial Conditions for Star Clusters. In *The Cambridge N-Body Lectures*; Aarseth, S.J., Tout, C.A., Mardling, R.A., Eds.; Springer: Berlin/Heidelberg, Germany, 2008; Volume 760, p. 181. [https://doi.org/10.1007/978-1-4020-8431-7\\_8](https://doi.org/10.1007/978-1-4020-8431-7_8).
8. Binney, J.; Tremaine, S. *Galactic Dynamics*; Princeton University Press: Princeton, NJ, USA, 1987.
9. Cowie, L.L.; Songaila, A.; Hu, E.M.; Cohen, J.G. New Insight on Galaxy Formation and Evolution From Keck Spectroscopy of the Hawaii Deep Fields. *Astron. J.* **1996**, *112*, 839. <https://doi.org/10.1086/118058>.
10. Thomas, D.; Maraston, C.; Bender, R.; Mendes de Oliveira, C. The Epochs of Early-Type Galaxy Formation as a Function of Environment. *Astron. J.* **2005**, *621*, 673–694. <https://doi.org/10.1086/426932>.
11. Recchi, S.; Calura, F.; Kroupa, P. The chemical evolution of galaxies within the IGIMF theory: The  $[\alpha/\text{Fe}]$  ratios and downsizing. *Astron. Astrophys.* **2009**, *499*, 711–722. <https://doi.org/10.1051/0004-6361/200811472>.
12. Thomas, D.; Maraston, C.; Schawinski, K.; Sarzi, M.; Silk, J. Environment and self-regulation in galaxy formation. *Mon. Not. R. Astron. Soc.* **2010**, *404*, 1775–1789. <https://doi.org/10.1111/j.1365-2966.2010.16427.x>.
13. McDermid, R.M.; Alatalo, K.; Blitz, L.; Bournaud, F.; Bureau, M.; Cappellari, M.; Crocker, A.F.; Davies, R.L.; Davis, T.A.; de Zeeuw, P.T.; et al. The ATLAS<sup>3D</sup> Project—XXX. Star formation histories and stellar population scaling relations of early-type galaxies. *Mon. Not. R. Astron. Soc.* **2015**, *448*, 3484–3513. <https://doi.org/10.1093/mnras/stv105>.
14. Yan, Z.; Jerabkova, T.; Kroupa, P. The star formation timescale of elliptical galaxies. Fitting  $[\text{Mg}/\text{Fe}]$  and total metallicity simultaneously. *Astron. Astrophys.* **2019**, *632*, A110. <https://doi.org/10.1051/0004-6361/201936636>.
15. Eappen, R.; Kroupa, P.; Wittenburg, N.; Haslbauer, M.; Famaey, B. The formation of early-type galaxies through monolithic collapse of gas clouds in Milgromian gravity. *Mon. Not. R. Astron. Soc.* **2022**, *516*, 1081–1093. <https://doi.org/10.1093/mnras/stac2229>.
16. Gjergo, E.; Kroupa, P. The impact of early massive galaxy formation on the cosmic microwave background. *Nucl. Phys. B* **2025**, *1017*, 116931. <https://doi.org/10.1016/j.nuclphysb.2025.116931>.
17. Weisz, D.R.; Dolphin, A.E.; Skillman, E.D.; Holtzman, J.; Gilbert, K.M.; Dalcanton, J.J.; Williams, B.F. The Star Formation Histories of Local Group Dwarf Galaxies. I. Hubble Space Telescope/Wide Field Planetary Camera 2 Observations. *Astrophys. J.* **2014**, *789*, 147. <https://doi.org/10.1088/0004-637X/789/2/147>.
18. McQuinn, K.B.W.; Skillman, E.D.; Cannon, J.M.; Dalcanton, J.; Dolphin, A.; Hidalgo-Rodríguez, S.; Holtzman, J.; Stark, D.; Weisz, D.; Williams, B. The Nature of Starbursts. I. The Star Formation Histories of Eighteen Nearby Starburst Dwarf Galaxies. *Astrophys. J.* **2010**, *721*, 297–317. <https://doi.org/10.1088/0004-637X/721/1/297>.
19. Haslbauer, M.; Yan, Z.; Jerabkova, T.; Gjergo, E.; Kroupa, P.; Zonoozi, A.H. The effect of the environment-dependent stellar initial mass function on the photometric properties of star-forming galaxies. *Astron. Astrophys.* **2024**, *689*, A221. <https://doi.org/10.1051/0004-6361/202347928>.
20. van Dokkum, P.G.; Abraham, R.; Merritt, A.; Zhang, J.; Geha, M.; Conroy, C. Forty-seven Milky Way-sized, Extremely Diffuse Galaxies in the Coma Cluster. *Astrophys. J. Lett.* **2015**, *798*, L45. <https://doi.org/10.1088/2041-8205/798/2/L45>.

21. Bullock, J.S.; Boylan-Kolchin, M. Small-Scale Challenges to the  $\Lambda$ CDM Paradigm. *Annu. Rev. Astron. Astrophys.* **2017**, *55*, 343–387. <https://doi.org/10.1146/annurev-astro-091916-055313>.
22. Milgrom, M. A modification of the Newtonian dynamics as a possible alternative to the hidden mass hypothesis. *Astrophys. J.* **1983**, *270*, 365–370. <https://doi.org/10.1086/161130>.
23. McGaugh, S.S.; Schombert, J.M.; Bothun, G.D.; de Blok, W.J.G. The Baryonic Tully-Fisher Relation. *Astrophys. J. Lett.* **2000**, *533*, L99–L102. <https://doi.org/10.1086/312628>.
24. Lelli, F.; McGaugh, S.S.; Schombert, J.M.; Pawlowski, M.S. One Law to Rule Them All: The Radial Acceleration Relation of Galaxies. *Astrophys. J.* **2017**, *836*, 152. <https://doi.org/10.3847/1538-4357/836/2/152>.
25. McGaugh, S.S. The Baryonic Tully-Fisher Relation of Gas-rich Galaxies as a Test of  $\Lambda$ CDM and MOND. *Astron. J.* **2012**, *143*, 40. <https://doi.org/10.1088/0004-6256/143/2/40>.
26. Bekenstein, J.; Milgrom, M. Does the missing mass problem signal the breakdown of Newtonian gravity? *Astrophys. J.* **1984**, *286*, 7–14. <https://doi.org/10.1086/162570>.
27. Milgrom, M. Generalizations of quasilinear MOND. *Phys. Rev. D* **2023**, *108*, 084005. <https://doi.org/10.1103/PhysRevD.108.084005>.
28. Scherer, D.; Pflamm-Altenburg, J.; Kroupa, P.; Gjergo, E. The p-Laplacian as a framework for generalizing Newtonian gravity and Milgromian gravitation. *Astron. Astrophys.* **2025**, *698*, A167. <https://doi.org/10.1051/0004-6361/202554793>.
29. Milgrom, M. Solutions for the Modified Newtonian Dynamics Field Equation. *Astrophys. J.* **1986**, *302*, 617. <https://doi.org/10.1086/164021>.
30. Hernquist, L. An Analytical Model for Spherical Galaxies and Bulges. *Astrophys. J.* **1990**, *356*, 359. <https://doi.org/10.1086/168845>.
31. Cappellari, M.; Emsellem, E.; Krajnović, D.; McDermid, R.M.; Scott, N.; Verdoes Kleijn, G.A.; Young, L.M.; Alatalo, K.; Bacon, R.; Blitz, L.; et al. The ATLAS<sup>3D</sup> project - I. A volume-limited sample of 260 nearby early-type galaxies: Science goals and selection criteria. *Mon. Not. R. Astron. Soc.* **2011**, *413*, 813–836. <https://doi.org/10.1111/j.1365-2966.2010.18174.x>.
32. Lelli, F.; McGaugh, S.S.; Schombert, J.M. SPARC: Mass Models for 175 Disk Galaxies with Spitzer Photometry and Accurate Rotation Curves. *Astron. J.* **2016**, *152*, 157. <https://doi.org/10.3847/0004-6256/152/6/157>.
33. Binney, J.; Tremaine, S. *Galactic Dynamics: Second Edition*; Princeton University Press: Princeton, NJ, USA, 2008.
34. Dabringhausen, J.; Hilker, M.; Kroupa, P. From star clusters to dwarf galaxies: The properties of dynamically hot stellar systems. *Mon. Not. R. Astron. Soc.* **2008**, *386*, 864–886. <https://doi.org/10.1111/j.1365-2966.2008.13065.x>.
35. Meylan, G.; Heggie, D.C. Internal dynamics of globular clusters. *Astron. Astrophys. Rev.* **1997**, *8*, 1–143. <https://doi.org/10.1007/s001590050008>.
36. Famaey, B.; McGaugh, S.S. Modified Newtonian Dynamics (MOND): Observational Phenomenology and Relativistic Extensions. *Living Rev. Relativ.* **2012**, *15*, 10. <https://doi.org/10.12942/lrr-2012-10>.
37. Sanders, R.H. Forming galaxies with MOND. *Mon. Not. R. Astron. Soc.* **2008**, *386*, 1588–1596. <https://doi.org/10.1111/j.1365-2966.2008.13140.x>.
38. Kroupa, P.; Jerabkova, T.; Thies, I.; Pflamm-Altenburg, J.; Famaey, B.; Boffin, H.M.J.; Dabringhausen, J.; Beccari, G.; Prusti, T.; Boily, C.; et al. Asymmetrical tidal tails of open star clusters: Stars crossing their cluster’s práh challenge Newtonian gravitation. *Mon. Not. R. Astron. Soc.* **2022**, *517*, 3613–3639. <https://doi.org/10.1093/mnras/stac2563>.
39. McGaugh, S.; Milgrom, M. Andromeda Dwarfs in Light of MOND. II. Testing Prior Predictions. *Astrophys. J.* **2013**, *775*, 139. <https://doi.org/10.1088/0004-637X/775/2/139>.
40. Misgeld, I.; Hilker, M. Families of dynamically hot stellar systems over 10 orders of magnitude in mass. *Mon. Not. R. Astron. Soc.* **2011**, *414*, 3699–3710. <https://doi.org/10.1111/j.1365-2966.2011.18669.x>.
41. Cappellari, M.; Scott, N.; Alatalo, K.; Blitz, L.; Bois, M.; Bournaud, F.; Bureau, M.; Crocker, A.F.; Davies, R.L.; Davis, T.A.; et al. The ATLAS<sup>3D</sup> project-XV. Benchmark for early-type galaxies scaling relations from 260 dynamical models: Mass-to-light ratio, dark matter, Fundamental Plane and Mass Plane. *Mon. Not. R. Astron. Soc.* **2013**, *432*, 1709–1741. <https://doi.org/10.1093/mnras/stt562>.
42. McGaugh, S.S.; de Blok, W.J.G. Gas Mass Fractions and the Evolution of Spiral Galaxies. *Astrophys. J.* **1997**, *481*, 689–702. <https://doi.org/10.1086/304100>.
43. Kennicutt, Jr., R.C. The Global Schmidt Law in Star-forming Galaxies. *Astrophys. J.* **1998**, *498*, 541–552. <https://doi.org/10.1086/305588>.
44. Leroy, A.K.; Walter, F.; Brinks, E.; Bigiel, F.; de Blok, W.J.G.; Madore, B.; Thornley, M.D. The Star Formation Efficiency in Nearby Galaxies: Measuring Where Gas Forms Stars Effectively. *Astron. J.* **2008**, *136*, 2782–2845. <https://doi.org/10.1088/0004-6256/136/6/2782>.
45. Hunter, D.A.; Elmegreen, B.G. Star Formation Properties of a Large Sample of Irregular Galaxies. *Astron. J.* **2004**, *128*, 2170–2205. <https://doi.org/10.1086/424615>.

46. Weisz, D.R.; Dalcanton, J.J.; Williams, B.F.; Gilbert, K.M.; Skillman, E.D.; Seth, A.C.; Dolphin, A.E.; McQuinn, K.B.W.; Gogarten, S.M.; Holtzman, J.; et al. The ACS Nearby Galaxy Survey Treasury. VIII. The Global Star Formation Histories of 60 Dwarf Galaxies in the Local Volume. *Astrophys. J.* **2011**, *739*, 5. <https://doi.org/10.1088/0004-637X/739/1/5>.
47. Bell, E.F.; de Jong, R.S. Stellar Mass-to-Light Ratios and the Tully-Fisher Relation. *Astrophys. J.* **2001**, *550*, 212–229. <https://doi.org/10.1086/319728>.
48. Gallazzi, A.; Charlot, S.; Brinchmann, J.; White, S.D.M.; Tremonti, C.A. The ages and metallicities of galaxies in the local universe. *Mon. Not. R. Astron. Soc.* **2005**, *362*, 41–58. <https://doi.org/10.1111/j.1365-2966.2005.09321.x>.
49. van Dokkum, P.G.; Whitaker, K.E.; Brammer, G.; Franx, M.; Kriek, M.; Labbé, I.; Marchesini, D.; Quadri, R.; Bezanson, R.; Illingworth, G.D.; et al. The Growth of Massive Galaxies Since  $z = 2$ . *Astrophys. J.* **2010**, *709*, 1018–1041. <https://doi.org/10.1088/0004-637X/709/2/1018>.
50. Banik, I.; Zhao, H. From Galactic Bars to the Hubble Tension: Weighing Up the Astrophysical Evidence for Milgromian Gravity. *Symmetry* **2022**, *14*, 1331. <https://doi.org/10.3390/sym14071331>.
51. Disney, M.J.; Romano, J.D.; Garcia-Appadoo, D.A.; West, A.A.; Dalcanton, J.J.; Cortese, L. Galaxies appear simpler than expected. *Nature* **2008**, *455*, 1082–1084. <https://doi.org/10.1038/nature07366>.
52. Feng, J.Q. Rotating Disk Galaxies without Dark Matter Based on Scientific Reasoning. *Galaxies* **2020**, *8*, 9. <https://doi.org/10.3390/galaxies8010009>.
53. Hofmeister, A.M.; Criss, R.E. Debate on the Physics of Galactic Rotation and the Existence of Dark Matter. *Galaxies* **2020**, *8*, 54. <https://doi.org/10.3390/galaxies8030054>.
54. Hofmeister, A.M.; Criss, R.E. Debated Models for Galactic Rotation Curves: A Review and Mathematical Assessment. *Galaxies* **2020**, *8*, 47. <https://doi.org/10.3390/galaxies8020047>.
55. Seth, A.C.; van den Bosch, R.; Mieske, S.; Baumgardt, H.; Brok, M.D.; Strader, J.; Neumayer, N.; Chilingarian, I.; Hilker, M.; McDermid, R.; et al. A supermassive black hole in an ultra-compact dwarf galaxy. *Nature* **2014**, *513*, 398–400. <https://doi.org/10.1038/nature13762>.
56. Mahani, H.; Zonoozi, A.H.; Haghi, H.; Jeřábková, T.; Kroupa, P.; Mieske, S. Do ultracompact dwarf galaxies form monolithically or as merged star cluster complexes? *Mon. Not. R. Astron. Soc.* **2021**, *502*, 5185–5199. <https://doi.org/10.1093/mnras/stab330>.
57. Hertzprung, E. Über die photographische Schwärzungskurve. *Astron. Nachrichten* **1911**, *190*, 119. <https://doi.org/10.1002/asna.19111900704>.
58. Russell, H.N. Relations Between the Spectra and Other Characteristics of the Stars. *Pop. Astron.* **1914**, *22*, 331–351.
59. Zhang, D.; Zonoozi, A.H.; Kroupa, P. Revisiting the missing mass problem in MOND for nearby galaxy clusters. *Phys. Rev. D* **2026**, *113*, 043027. <https://doi.org/10.1103/mp3f-q5dc>.

**Disclaimer/Publisher’s Note:** The statements, opinions and data contained in all publications are solely those of the individual author(s) and contributor(s) and not of MDPI and/or the editor(s). MDPI and/or the editor(s) disclaim responsibility for any injury to people or property resulting from any ideas, methods, instructions or products referred to in the content.